Fluctuations, Line Tensions, and Correlation Times of Islands on Surfaces

F. Szalma[1, 2, *] and T.L. Einstein[1, †]

[1] Department of Physics, University of Maryland, College Park MD 20742-4111
[2] Institute of Theoretical Physics, Szeged University, H-6720 Szeged, Hungary
(Dated: February 12, 2004)

We analyze in detail the fluctuations of the (spatial) Fourier modes of nano-scale islands using kinetic Monte Carlo simulations with realistic energy barriers for hopping rates. From the analyses of the fluctuation of each individual mode we deduce absolute line tensions in the azimuthal directions of the surface. We show that the coupling of the modes due to the anisotropy of a crystal surface does not affect the fluctuations in the anticipated way. The autocorrelation functions of these modes give the scaling of the correlation times with wavelength in the experimentally observed regime. Both the energetic parameters and the correlation times give very good agreement with available experimental data and also provide a tool to extrapolate to much more complex structures than used in these MC simulations.

arXiv:cond-mat/0312621 v2   11 Feb 2004

I. INTRODUCTION

Nanoscale islands consisting of $10^2 – 10^5$ atoms have captured great interest over recent years for a variety of reasons. From a practical standpoint, they provide a precursor to the formation of quantum dots, which, if assembled in a controlled way, can serve as the basic ingredients of nano-scale electronic and mechanical devices. Many crystallites or nanomounds are best viewed as "wedding-cake"-like stacks of such islands.[1] They are the intermediary between a flat surface and a small three-dimensional structure. In contrast to steps, which require vicinal surfaces[2] that often must be well characterized over mesoscopic regions, islands can be studied in smaller-scale regions that are flat only locally.

Of particular interest to us are the shape and the fluctuations of the perimeter of these islands. The shape provides information about the line tension or step free energy per length, from which one can compute the step stiffness that describes the "inertial" properties of steps. The "dipole" mode of these fluctuations are long known to underlie the diffusion of such islands, but shorter-wavelength modes are also of great interest, since they can be correlated with similar fluctuations of steps and provide a way to assess, again, the stiffness of the step and also the kinetic or atomistic diffusion coefficient associated with the mechanism that dominates the atomistic processes underlying the fluctuations. Until recently, attention was limited to structures for crystal anisotropy could seemingly be ignored.

Here we pay particular attention to the role of the inevitable anisotropy of crystal surfaces, which around room temperature or even above it is typically sufficiently strong that it should apparently be taken into account in order to correctly characterize the morphology of the various (near) equilibrium structures appearing on surfaces and their dynamics. In this paper we focus on the line tension and stiffness and their orientation dependence; we give an analytic method to calculating these physical parameters from the fluctuation of nanoscale islands.

The little experimental data on such systems involve runs of worrisome duration or use probes that provide scanned rather than instantaneous images. To generate fully-characterized data, we turned to kinetic Monte Carlo (KMC) simulations to mimic the equilibrium fluctuations of islands. These simulations are the input of our analytic theory which, starting from the excess free energy corresponding to the capillary wave fluctuations of the island edge, provides the *eigenmodes* of these fluctuations. Since the 2D Wulff plot relating the equilibrium island shape and the line tension in the azimuthal directions on the surface provides only *relative* line tensions for various orientations, a key problem is always the determination of the chemical potential λ of the island edge, which then produces an *absolute* relation. This potential can be determined with surprisingly good ($\sim 10\%$) accuracy from the spectrum of the modes of the system. We compare these eigenmodes and the simple Fourier modes of the fluctuations and reach the surprising conclusion that neglecting anisotropy in our case can actually improve results!

Another aim of the paper is to examine the correlation of the fluctuations of the Fourier modes and thereby to find the rate-limiting process driving the fluctuations in a fairly realistic model. For our KMC simulations we sought a system for which one could compute hop rates with good accuracy and for which there was quantitative experimental data with which to compare. Accordingly, we have chosen Pb(111) so as to be able to compare with intriguing recent experiments by Thürmer et al.[3] This analysis gives the scaling of the correlation time with the wavelength, that is the dynamic exponent z, and provides us with characteristic times measured not only in MC steps, but in *real* time. Thus, we can compare directly with experiments and extrapolate to different structures from the simple one considered here.

Utilizing direct surface imaging techniques, especially scanning tunneling microscopy (STM), several attempts have been made to measure and calculate step energies. From a theoretical viewpoint the various methods that
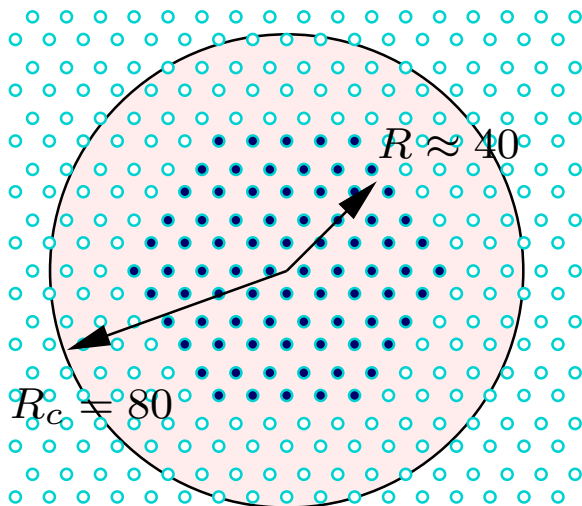
FIG. 1: Geometry of the MC simulation. The approximate mean radius R of the island and the radius R_c of the container are illustrated.

used the experimental data for calculations can be broken down into two main groups. The first is based on a lattice model which relates the island shape (radius and curvature) to the temperature dependence of the free energy and stiffness of the Ising model in the low-temperature expansion, usually in high symmetry directions. By fitting the functional shape of the free energy with varying temperature on the experimental data determined by the equilibrium island shape[4] gives the Ising kink energy, which in turn provides the step energies and stiffnesses. However, limitations of the Ising model to describe surface structure have recently been noted.[5]

The other method is based on a step continuum model which makes use of stochastic differential equations to describe the fluctuations of straight steps[6] or island edges[7,8] viewed as nearly circular closed-loop steps. Thus, the initial calculations for island fluctuations assumed isotropy:[9] the power spectrum of the Fourier modes of the step fluctuations were calculated and adapted with appropriate modifications to nearly circular island shapes.[10] If the anisotropy turns out to be strong, it cannot be handled as a perturbation; a complete anisotropic calculation without any such assumptions becomes necessary.

This challenge was recently been taken up by Khare et al.,[11] who give an approximate form for the free energy functional and calculate the chemical potential integrating all the Fourier modes in the system by using the generalized equipartition theorem where the modes are buried in a sum. However, these modes are coupled, so any one mode missing (e.g. due to lack of experimental resolution) in the sum can contribute to a deviation from the precise value of the chemical potential by itself and through its coupling to the other modes as well. In contrast, our approach of analyzing individual modes gives more insight into the extent to which this coupling should be taken into account and provides the chemical

potential in a (mathematically) controlled way.

The autocorrelation function of fluctuations of step edges and correlation times have been analyzed theoretically in Fourier space based on the Langevin formalism,[9,12] and in the context of straight-step fluctuations on Si(111)[13] and Si(001)[6] surfaces for relatively long wavelengths. The rate-limiting kinetics driving these fluctuations are determined by the dynamic exponent, which also sets the universality class to which the system belongs,[14] as the roughening exponent is always supposed to be $\alpha = 2$ in our cases. The correlation times are theoretically identical to the relaxation time (or elsewhere decay time) of surface features,[15,16] like decay and build-up of bumps and valleys in the step edge still near equilibrium, of a (wave)length L, and also that of three dimensional features like mesoscopic (or smaller) wires on surfaces and surface corrugations as in earlier studies by Mullins.[17,18]

The paper is organized as follows: In the next section we give an analytic solution to the decoupling of the Fourier modes of the system into the actual eigenmodes and recalculate the free energy functional of the edge fluctuations. The results can be understood without the reader's going through this algebra, only the result, expressed in Eq. (10), is used later. In Sec. III we introduce the KMC simulation and in Sec. IV use its results to calculate the chemical potential and line tension. In Sec. V we calculate the correlation functions of the Fourier modes and deduce the scaling of the correlation time with length, the dynamic exponent z. We compare with available experimental data. Sec. VI concludes the paper.

II. FOURIER MODES, EIGENMODES

The relationship between the equilibrium crystal shape and the surface tension or, in our 2D case, between the equilibrium island shape and the line tension of its edge can be established by the minimization of the free energy functional of the island edge. The orientation-dependent line tension $\beta(\mathbf{n})$ is defined as the work per unit length necessary to create the ds line element with normal $\mathbf{n}$ to the perimeter. The free energy is the integral of this work along the whole perimeter. The equilibrium island shape at a constant temperature T, number of particles N, and area Σ, is determined by the minimization of the free energy functional with respect to the shape with the constraint that the island area is constant, typically using the method of Lagrange multipliers:[19]

$$F[R, \dot{R}, \theta] = \oint_{L_{eq}} \beta(\mathbf{n})ds - \lambda \int_{\Sigma} d\sigma =$$
$$= \int_0^{2\pi} \beta(\psi(\theta)) \left(R^2 + \dot{R}^2 \right)^{1/2} d\theta - \lambda \int_0^{2\pi} \frac{R^2}{2} d\theta. \quad (1)$$
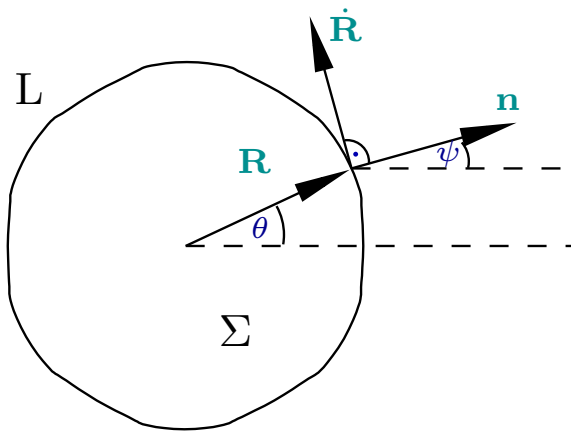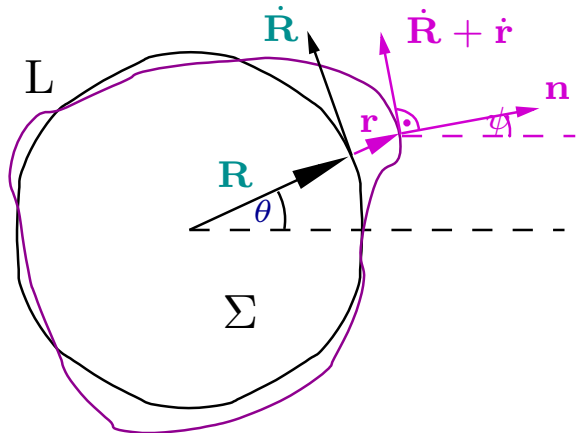
FIG. 2: Equilibrium island shape

FIG. 3: Instantaneous island shape. For a particular azimuthal direction, θ, the deviation from the equilibrium island shape, r, its derivative with respect to θ, $\dot{r}$, the unit vector normal to the instantaneous shape, $\mathbf{n}$, and the corresponding angle, ψ, are all time dependent.

Here the second line is in polar coordinates with θ the polar angle and $R(\theta)$ the radius of the equilibrium shape. The dot denotes the differentiation with respect to the angle, λ is the Lagrange multiplier (which actually turns out to be the chemical potential), and ψ is the angle which characterizes the vector normal to the shape (see Fig. 2). ds and $d\sigma$ are the line element and surface element, respectively. Formally minimizing the $F = F[R, \dot{R}, \theta]$ functional, the Euler-Lagrange equation gives a relation between the equilibrium island shape $R(\theta)$ and the orientation dependent line tension, $\beta(\psi)$, and between the two angles involved: ψ which depends on the polar angle and the equilibrium shape.[11,20]

$$\frac{\delta F}{\delta R} = 0 \implies \begin{array}{l} \beta(\psi) = \lambda \dfrac{R^2}{\left(R^2 + \dot{R}^2\right)^{1/2}} \\ \psi = \theta - \arctan \dfrac{\dot{R}}{R} \end{array} \quad (2)$$

However, in this procedure λ is a prefactor and cannot be determined, leaving the relation relative. Eq. (2) is the seminal Wulff construction in polar coordinates.

In order to determine the chemical potential, the thermal fluctuations of the island edge can be utilized. In this case the free energy of the island changes as its shape changes due to the fluctuations, and the free energy is certainly not at its minimum but depends on the island's instantaneous shape. Then the free energy of this instantaneous shape is the integral over the line elements of the shape with their corresponding line tension, which changes with time as the orientation of the shape element changes:

$$\begin{aligned} F[r, \dot{r}, \theta; t] &= \oint_L \beta(\mathbf{n}) ds = \\ &= \int_0^{2\pi} \beta(\psi(\theta)) \left((R+r)^2 + (\dot{R}+\dot{r})^2\right)^{1/2} d\theta \end{aligned} \quad (3)$$

Here r and $\dot{r}$ are time dependent and describe the deviation of the instantaneous shape from the equilibrium one

as shown in Fig. 3. The angle ψ is also time-dependent since now it depends not only on R and $\dot{R}$ as in Eq. (2), but also on r and $\dot{r}$. Considering only small deformations from the equilibrium shape (as it is usually assumed in the capillary wave theory) and also small slope deviations from the equilibrium slope $\dot{R}$, so that $r, \dot{r} \ll R$, the Taylor expansion (both in β and in the square root) in these small parameters leads to the functional

$$F[r, \dot{r}, \theta; t] = \lambda \int_0^{2\pi} \frac{1}{2} \frac{\left(\dot{R}r - R\dot{r}\right)^2}{R^2 + 2\dot{R}^2 - R\ddot{R}} d\theta. \quad (4)$$

This functional contains 3 quadratic terms $A(\theta)r^2$, $Q(\theta)r\dot{r}$ and $B(\theta)\dot{r}^2$. The cross term Q drops out after taking the ensemble average; both the two other terms are determined by properties of the equilibrium island shape:

$$A(\theta) = \frac{1}{2} \frac{\dot{R}^2}{R^2 + 2\dot{R}^2 - R\ddot{R}} \quad (5)$$

$$B(\theta) = \frac{1}{2} \frac{R^2}{R^2 + 2\dot{R}^2 - R\ddot{R}}, \quad (6)$$

and provide the weightings of the fluctuations of the deformations characterized by r^2 and $\dot{r}^2$, respectively. These deformations at the microscopic level are due to the thermal movement of adatoms surrounding the island constantly attaching to its edge and coming off from it.

To diagonalize the free energy one rewrites the integrand in Fourier form

$$F[\{r_n\}; t] = 2\pi\lambda \sum_{m,n} (A_{m-n} + mnB_{m-n}) r_n(t)r_m^*(t), \quad (7)$$

where $r_k = \int_0^{2\pi} r(\theta) \exp[ik\theta] d\theta$ and similarly for A_k and B_k. The Fourier modes are coupled due to the anisotropy,

which is contained in A and B as we shall see shortly. Here $n = 0$ is the expansion-contraction mode; $n = 1$, which we called the dipole mode in the Introduction, is related to the Brownian, diffusive motion of the island; $n = 2$ is a quadrupolar distortion, i.e. an elongated shape with two maxima and two minima in perpendicular directions; and so on. The Fourier components have hermitian properties since $A(\theta)$ and $B(\theta)$, the factors associated with the equilibrium island shape, are real functions; hence, $A_{-i} = A_i^*$, $B_{-i} = B_i^*$, and $r_{-i} = r_i^*$.

The free energy of Eq. (7) can readily be cast into matrix form:

$$F[\mathbf{r}; t] = 2\pi\lambda\mathbf{r}^\dagger \left(\mathbf{A} + \mathbf{MBN}\right)\mathbf{r} \ , \qquad (8)$$

where $\mathbf{r}$ is a vector containing the Fourier components of the instantaneous island shape, $\mathbf{A}$ and $\mathbf{B}$ are hermitian matrices, $[\mathbf{A}]_{m,n} = A_{m-n}$, $[\mathbf{B}]_{m,n} = B_{m-n}$, and $\mathbf{M} = \mathbf{N}$ are diagonal matrices with the wavenumbers along the diagonal.

As in practice there are only a finite number of atoms on the edge of the island, we discretize the problem. If the number of atoms on the edge is $2N$, there are as many modes in the system; as we will see in Sec. IV, to analyze the right number of modes is crucial to the problem. Now, if $\mathbf{r}$ contains the r_k Fourier components from $-N + 1$ through N, the Fourier transform is discrete and $r_k = \sum_{j=-N+1}^{N} r_j^\theta \exp[i\,k\,j\pi/N]$, where r_j^θ is the deviation from the equilibrium shape in the $\theta = j\pi/N$ direction.

The A_k and the B_k can be obtained similarly; and $\mathbf{A}$ and $\mathbf{B}$ are finite cyclic hermitian matrices, meaning that their diagonal elements are the same. They also reflect the symmetry of the equilibrium shape as e.g. in our case due to the six-fold symmetry the principal diagonal is filled with A_0, the 6th to the right with A_{-6}, etc. As $\mathbf{M}$ and $\mathbf{N}$ are the same diagonal matrices, the $\mathbf{MBN}$ product keeps the hermitian property.

In the isotropic case (when the equilibrium shape is circular), $A(\theta) = 0$ and $B(\theta) = 1/2$ for all θ. After the Fourier transformation this gives $\mathbf{A} = 0$ (zero matrix) and $\mathbf{B} = (1/2)\mathbb{1}$ (diagonal matrix). The anisotropy comes into play when the equilibrium shape is not circular, so that $A(\theta)$ and $B(\theta)$ are not constants and their higher order Fourier components fill the (off-)diagonals. These off-diagonals couple the Fourier modes.

Due to hermiticity the above matrix form is diagonalizable

$$F[\{h_n\}; t] = 2\pi\lambda \sum_n \Lambda_n h_n h_n^* \ , \qquad (9)$$

and the eigenvalues Λ_n of the $\mathbf{A} + \mathbf{MBN}$ matrix are all real. As we see shortly (in Eq. (10)) these eigenvalues are related to the strengths of the h_n eigenmodes, which at every time instant are just the transforms of the $r_n(t)$ Fourier modes of the instantaneous island shape. Again due to hermiticity, there is a unitary matrix $\mathbf{U}$ which

transforms Eq. (8) into Eq. (9) and gives the linear relationship between $\mathbf{r}$ and $\mathbf{h}$: $\mathbf{r} = \mathbf{Uh}$, where the vector $\mathbf{h}$ contains the h_n as its elements.

This decomposition of the free energy into eigenmodes in Eq. (9) facilitates the calculation of the Lagrange multiplier λ. In equilibrium, according to the equipartition theorem, the ensemble average of each mode, representing a degree of freedom, must have the same Boltzmann energy:

$$2\pi\lambda \overbrace{\Lambda_n \langle |h_n|^2 \rangle}^{E_n} = \frac{1}{2}k_B T. \qquad (10)$$

Λ_n and $\langle |h_n|^2 \rangle$ can be determined from the equilibrium island shape and the fluctuating island perimeter, respectively. Here E_n must be a constant in n, the modes, as the temperature and the chemical potential, λ, are fixed macroscopic parameters of the island. From this equation one can determine the same λ, in principle, from any mode. Thus, either experimentally observing island fluctuations or using Monte Carlo simulations one can determine E_n, which in turn provides λ. This λ was the missing parameter to determine *absolute* line tensions, and plugging it back into Eq. (2), we get the line tension in all azimuthal directions.

III.   KINETIC MONTE CARLO

The scarcity of extensive experimental data leads us to use Monte Carlo methods to simulate the behavior of the system. Another advantage of computer simulations will also become clear in the next section: analyzing correlation times.

Since our original motivation was to simulate the relaxation of a Pb crystallite with a (111) facet, we place a nanoscale island on a triangular lattice. We surround it by a non-permeable circular container of radius R_c to let the system reach its thermodynamic equilibrium, in order to measure its equilibrium fluctuations.[21,22] Thus, this geometry corresponds to an island placed on top of a facet of a crystallite (with an infinite Ehrlich-Schwoebel barrier). Note that by adjusting the permeability one can tune the overall decay rate of the island, which in this paper we fix at zero.

Since the temperature of the systems of interest is low compared to the energy barriers of adatomic hopping, we have chosen to use the Bortz-Kalos-Lebovitz (BKL) continuous-time MC algorithm[23] as it is best suited to low temperature systems and as its rejection-free method allows us to greatly improve the efficiency of the simulations compared to traditional Metropolis algorithms. Using the n-fold way method to keep track of the available MC moves, we could improve the efficiency even further. Because of the small number of energy barriers, the n-fold way approach (6-fold) is superior to the binary tree implementation of the BKL algorithm.[24]

Process	Energy (meV)	Energy (K)	Trial energy (K)
Surface diffusion	70	812	700
Edge diffusion	110	1276	1400
Break 1 bond	220	2552	2800
Break 2 bonds	360	4176	5600
Break 3 bonds	470	5452	5600
Break 4,5 bonds	600	6960	5600
Attach			700
Out			70000

TABLE I: Tabulation of the 8 energy barriers used in KMC simulations of Pb(111). The energies in columns 2, 3 were computed by M. Haftel using SEAM[25] with glue potentials[26]. The trial energies are the ones actually used in the simulations.

The energy barriers for hopping rates are mainly based on the semiempirical embedded atom method (SEAM)[25] using Ercolessi's glue potentials for the Pb(111) surface.[26] As we are not interested in all the details of this surface in the simulations, but only try to capture the main mechanisms, we do not take into account the ABC structure of the fcc lattice of Pb(111). Hence, the top layer constitutes a triangular lattice with perfect six-fold symmetry. Since there are 8 nearest neighbors to the two sites involved in any hopping process, there are 2^8 different configurations and entries in our KMC look-up table. We had energy barriers calculated for 13 different hopping processes, with which we tried to find the main, markedly different processes, and compare them to a few others we suspected to be close to the main ones. In this way the main processes fall into 8 groups. The terrace diffusion barrier is the hopping barrier for adatoms with no nearest neighbors, the edge diffusion barrier is the energy barrier for adatom rolling along a step edge with a negative kink at its back, the "break 1 bond" barrier is e.g. rolling along the step edge with no kinks etc., there is an attachment barrier for adatoms which approach the step edge with no nearest neighbors, and a (very high) barrier that keeps adatoms from hopping out of the container. We simplified this scheme even further according to a simple pattern as can be seen in the last column of Table I. Thus, the energy barriers are closer to realistic ones than as if we had just used conventional bond counting.

The basic parameters of the surface investigated and the KMC simulations are: The nearest-neighbor spacing a_1 on the Pb(111) surface is 3.50Å. The typical island diameter $2R$ is 40 to 80 a_1, while the container diameter R_c ranges from 12.5% to 300% larger than the island. We examined temperatures 350K, 400K, and 500K. In each MC snapshot of the island, we measure the island radius from the instantaneous center of mass in 360 "equiangular" directions.

We start the simulations from a nearly circular shaped configuration and let it relax to equilibrium, starting the MC measurement of the fluctuation and shape after the longest wavelength mode has passed its correlation time.
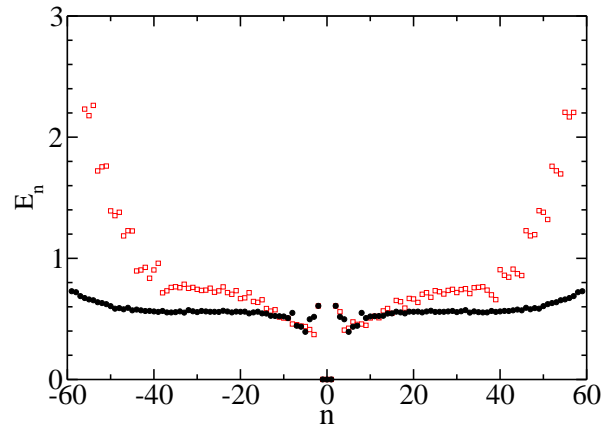

FIG. 4: Eigenmodes (open squares) and Fourier (solid circles) modes at $T=400$K, $R=20a_1$, $R_c=80a_1$. E_n is measured in atomic spacing units.

Especially for the lower temperatures, the typical equilibration times are very long, consistent with reports in other works.[27,28] Ensemble averages are taken from 100 to 3000 different runs starting from the same initial configuration, but with different random-number seeds. In each run, after equilibration, we get statistically independent fluctuations at time intervals again determined by the relaxation time of the longest wavelength mode. We take such independent "snapshots" of the islands 5 to 200 times in each run, so that we typically have 10,000 to 70,000 islands for taking averages.

IV. CHEMICAL POTENTIAL, LINE TENSION, LINE STIFFNESS

As described in detail in Sec. II, the energetic parameters of the island edge are determined by the island shape and its edge fluctuation. The Wulff construction provides the relationship between the relative line tension in the azimuthal directions on the crystal surface and the equilibrium island shape, and the information from the fluctuations $\langle |h_n|^2 \rangle$ of each mode in Eq. (10) gives the chemical potential λ that makes the Wulff construction absolute in Eq. (2).

From our KMC simulations we determine E_n of Eq. (10); it is depicted in Fig. 4 for $T=400$K and $R=20a_1$ island radius. Since the perimeter is about $120a_1$, we use 120 points to describe the circumference out of the 360 available.

We calculate E_n both using the transformation to the eigenmodes taking into account the anisotropy, and also pretending the islands were isotropic. In this latter case the $h_n = r_n$ are simply the Fourier modes, and $\Lambda_n = (1/2)n^2$.

The Fourier modes are fairly constant, as might be expected from equipartition for the isotropic case. However, we expect such a constant behavior after the transformation to the eigenmodes, but, instead, the transfor-

mation shifts E_n upward (cf. Fig. 4) and leads to greater scatter than found for the Fourier modes. This surprising observation suggests that for these islands the Fourier modes provide a better basis for chemical-potential calculations. Thus, determining E_n from the *Fourier* modes for intermediate wavenumbers, where the spectrum has a clear plateau, gives $E_n = 0.57a_1^2$ and through Eq. (10) and Eq. (2) $\beta = 26.2$ meV/Å for the line tension for the high-symmetry direction. This value well approximates the experimentally obtained ones for Pb(111) at T=393 K: $\beta_{1A} = 27.9$ meV/Å and $\beta_{1B} = 26.5$ meV/Å for A- and B-type steps, respectively.[29] In our simulations the two directions corresponding to the two different types of steps are intrinsically equivalent because we assume six-fold symmetry as the available values for energy barriers that we use in our KMC do not distinguish between the A- and B-directions, as mentioned in Sec. III.

At higher temperatures the eigenmodes and the Fourier modes come closer together, as one would expect since the equilibrium shape is more nearly circular and less affected by the underlying anisotropy, while at lower temperatures the eigenmodes are shifted more than in Fig. 4 compared to the Fourier modes (which still give a nice constant for E_n), and are even fuzzier.

In earlier works[11,20] where experimental data are used as an input of similar calculations, there is a sum over the modes, but because those modes are buried in a sum in the generalized equipartition theorem, one cannot see whether they are the modes which satisfy, at least to a certain extent, the equipartition theorem. Such experimental data may suffer from other problems which we mention in the next section.

For the same temperature but larger system sizes, $R=40a_1$ and $R_c=80a_1$, the Fourier modes are depicted in Fig. 5. In this case there are about 240 atoms on the perimeter. Since we cannot divide the 360 perimeter points into 240 equiangular ones to make Fourier transforms, we approximate it by N=180 or N=360 and observe how the plateau changes from what we saw in Fig. 4. The comparison of these two plots from MC simulations might help analyzing experimental data with limited resolution as well, as it shows how the Fourier modes behave in case of undersampling ($N=180$) and oversampling ($N=360$). The undersampled modes give higher values for E_n than expected for modes $|n| > 30$, as if those modes took over the energy of the modes that are missing (namely $180 < |n| \leq 240$) in the spectrum. When oversampled there is not enough energy for all modes in the sampling, so they go below the expected value of E_n. This is the simple reason of the peculiar shape of the two curves in Fig. 5 The value of E_n can still be determined quite accurately from where the two curves start to separate, providing $E_n = 1.22a_1^2$ which in turn gives $\beta = 24.6$ meV/Å , again in the range of the available experimental data.

From the equilibrium island shape using the Wulff construction, we have determined the relative line tensions in the azimuthal directions on the (111) surface (see Fig.
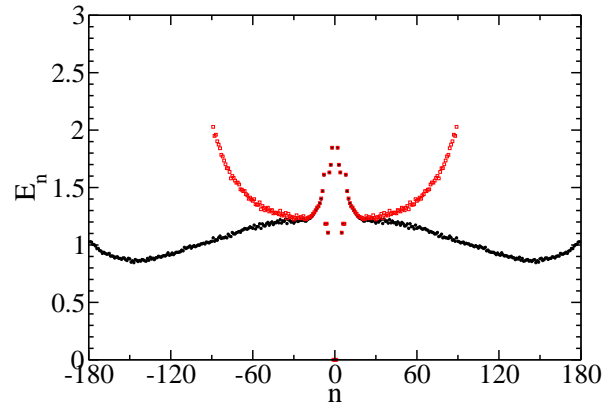

FIG. 5: Fourier modes for N=180 points (open squares) and N=360 points (solid circles) on the perimeter modes at T=400K, and R=$40a_1$, R_c=$80a_1$. E_n is measured in atomic spacing units.

6). The equilibrium shape is almost faceted in the six main directions, so the stiffness (not shown in the figure) spikes out very much. This effect might be a peculiarity of the KMC simulation since we take into account only a small subset of energy barriers of adatom hops. Thus, we lose subtle features such as the exact curvature especially when it is almost singular. In terms of the Wulff plot, cusp-like points are then hard to resolve in such simplified models. The limited statistics that could be reached (see the next section and Ref. 28 for reasons) have been a strong limiting factor as well.
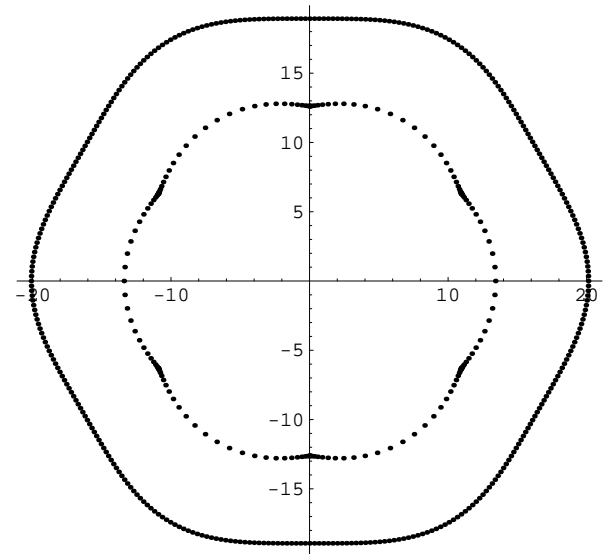

FIG. 6: Polar plot of the equilibrium island shape $R(\theta)$ (outer dots) and the relative line tension $\beta(\psi)$ (inner dots) in arbitrary units at T =400K, R=$20a_1$, R_c=$80a_1$.

V. AUTOCORRELATIONS, CORRELATION TIMES, KINETICS

Inspecting the autocorrelation functions in Fourier space, the longest wavelengths have surprisingly long correlation times (in CPU time), which made the full equilibration of these fairly large (at least for the computer) systems very hard to reach in order to make MC measurements in equilibrium. Most surprising is that the islands relax to their equilibrium shape 10 to 100 times faster than the longest-wavelength modes. Hence, estimating the thermalization time from just the shape relaxation may be very misleading and can give problematic results not characteristic of equilibrium. Such behavior may include fake, strong mode coupling, or stronger fluctuations in autocorrelation functions even in case of good statistics. To get the following results it was necessary to have a highly-optimized code.

The temporal correlations can be characterized by

$$G(t) = \left\langle [r(t_0) - r(t_0 + t)]^2 \right\rangle \propto t^{1/z}. \qquad (11)$$

As we measure correlations in equilibrium, t_0 must be greater than the thermalization time of the system. Here $r(t)$ is the fluctuation from the equilibrium shape, as before, and depends on the angle, θ, and time. The average is taken over angles and an ensemble as well. The angular averaging is strictly valid only for the isotropic case, but the results of the previous section imply that it is adequate in our case.

The typical behavior of the correlation function is that the exponent, $1/z$, remains at 1 for very short times[27] and then crosses over to a value which characterizes the rate-limiting kinetics driving the fluctuations of the island edge; eventually it crosses over to zero if the system is finite as this correlation function saturates.

Pure rate-limiting kinetics have been thoroughly investigated[9,12,30,31,32], and the dynamic exponent, z, in these well-defined cases can take the values 2 for attachment-detachment kinetics, 3 for terrace diffusion, and 4 for step-edge diffusion, where the last mechanism gives a very slow dynamics. There can be crossover regimes between these pure cases, leading to values of z between the quoted values, and certain geometries can also effect the value of z. One should also see crossovers as length scales vary.[9,12,32]

To investigate the length-scale dependence of the correlation function, it is more appropriate to use the correlation function in Fourier space.

$$G_n(t) = \left\langle |r_n(t_0) - r_n(t_0 + t)|^2 \right\rangle \qquad (12)$$

$$= C_n \left(1 - \exp\left(-|t|/\tau_n\right)\right), \qquad (13)$$

where the C_n are twice the amplitudes of the fluctuations of the modes, as analyzed in the previous section, and the τ_n are their correlation times. The wavenumber dependence of τ_n is known to have an intimate relationship
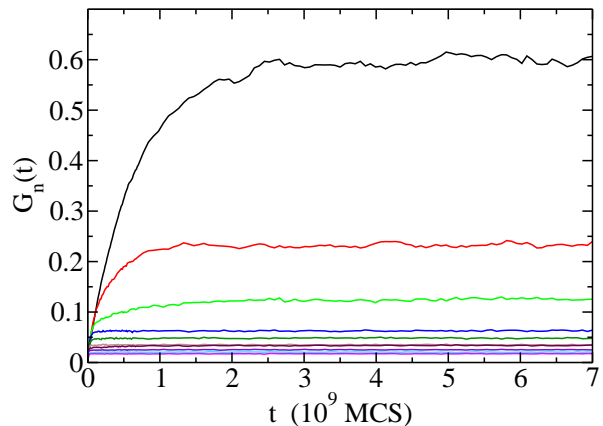

FIG. 7: Correlation function $G_n(t)$ of the Fourier modes for n=2,...,10 from top to bottom. T =400K, R=20a_1, R_c=80a_1.

with the exponent in $G(t)$, namely

$$\tau_n \sim n^{-z}. \qquad (14)$$

Thus, the correlation time increases with increasing wavelength, with the scaling exponent z. For larger exponent z, the correlation times grow more rapidly, so that for longer wavelengths the correlations and the dynamics in general can slow down very quickly.

Here we pay particular attention to the longest wavelength and its corresponding correlation time τ_2, which makes the largest contribution to the fluctuations and relaxes the most slowly. From the wavelength dependence of the correlation time we also determine the dynamic exponent and the rate limiting kinetics.

In the KMC simulations for T=400K and R=20a_1, the longest-wavelength mode, n=2, is 120a_1 or 420Å long. From Fig. 7, its relaxation time is $\tau_2 = 6.7 \times 10^8$ MCS (Monte Carlo steps). To give a crude estimate for τ_2 in real time, we consider the hopping rate

$$\nu = \nu_D \exp[-\beta E_b] \qquad (15)$$

to be the product of the attempt frequency, which we identify with the Debye frequency of Pb: $\nu_D = 1.83 \times 10^{12}$ Hz,[33] and the Boltzmann factor of the energy barrier of a particular hop. Hence, a MCS in this Monte Carlo simulation is equivalent to a $1/\nu_D$ time increment in *real* time; thus, the relaxation time in this particular case is $\tau_2 = 0.37$ msec.

For R=40a_1 the n=2 mode is twice as long: 240a_1 or 840Å. Its relaxation time is approximately 8 times as large, 4.5×10^9 MCS or 2.5 msec.

As expected, these correlation times change dramatically with temperature as the underlying physical phenomena are activated. For R=40a_1 at T=350K, $\tau_2 = 4.8 \times 10^{10}$ MCS or 26.4 msec, which means 10 times slower relaxation compared to 400 K, while for 500 K $\tau_2 = 3 \times 10^8$ MCS or 0.16 msec, which represents 20 times faster behavior than for 400 K.

The scaling of the relaxation time with (wave)length can be seen in Fig. 8. In the plotted wavenumber range, overall, τ_n behaves like $z = 3$ or 4 suggesting that the mechanism driving the fluctuations is step-edge diffusion[34,35] or the system is in a crossover region between terrace diffusion and step-edge diffusion. The apparent wiggle might be a precursor of an oscillatory behavior of the relaxation-time scaling with the wave number and is most probably due to the anisotropy or simply the geometry of the system as it seems characteristic independent of system sizes. In our case, due to the six-fold symmetry, the periodicity should be $\Delta n = 6$. This implies that it is not an oscillation between different rate limiting behaviors for different wavelengths.

Comparison of these length scales and their corresponding relaxation times with existing experimental observations might give interesting physical insight. For example, in the experiment by Thürmer et al.,[3] a small Pb crystallite slightly larger than 1 μm relaxes at 383K to its equilibrium (or at least steady-state) shape in 1-2 days after being quenched from a higher temperature. Assuming that the higher temperature thermodynamically "drives" the system only marginally out of its equilibrium state at 383K, the post-quench relaxation should respond to the same thermodynamic forces as those producing the fluctuations of the perimeter of a single-layer island as considered so far; the relaxation time of the structure can then be readily evaluated based on the above arguments. Since the crystallite is 50 times larger than the longest wavelengths in our KMC simulations for the larger system size, the relaxation time is 1.25×10^5 times longer if the kinetics to be rate-limited by terrace diffusion. Alternatively, τ_{relax} is 6.25×10^6 times longer if the kinetics to be rate-limited by step-edge diffusion (though, of course, attachment-detachment and terrace diffusion could be present but NOT rate-limiting). Specifically, these values of τ_{relax} are 312 sec and 4.3 h, respectively, based on our KMC data at T=400K. As the actual temperature of the experiment was lower than this, the extrapolated KMC data are in remarkably good agreement with the experimental time range.

The above arguments lead to a general view of the evolution of surface structures. For Pb in the temperature range 350 K–400 K, one observes the slow development and relaxation of fluctuations at the μm scale in experiments. Assuming that the rate-limiting kinetics retain the same z =3, 4 range for even longer wavelengths, structures of 10 μm size — step edges, islands, etc. — take years to change, so in effect they look frozen under laboratory conditions. This is the reason why structures do not show any changes on the large scale at lower temperatures while on a shorter scale they can be very active.

Lowering the temperature makes the length scales — at which evolution or relaxation can be observed — exponentially shorter, which is readily understandable if one looks at the converse of the above arguments. The length scales with time like $l \sim \tau^{-1/4}$ (for $z = 4$) whereas τ scales like $1/\nu$ in Eq. (15). Thus, the length scales
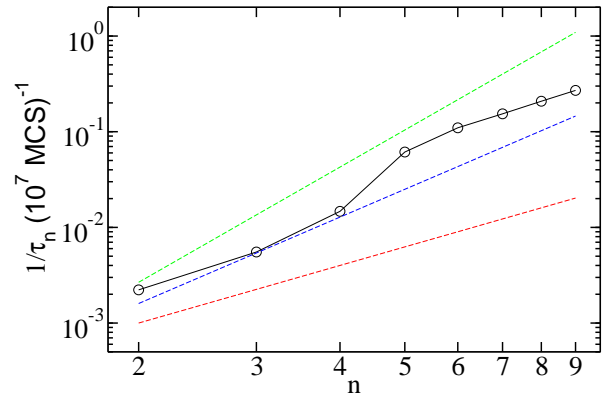

FIG. 8: Correlation time τ_n vs. wave number n on a log-log scale. The MC data (black circles) show a $z = 4$ step-edge diffusion or $z = 3$ terrace diffusion kinetics as an overall behavior in this wave number range. The dashed lines represent z=4, 3, and 2 (from top to bottom) dynamic exponents. T =400K, R=40a_1, R_c=80a_1.

with temperature like $l \sim \exp\left[E_b/4k_BT\right]$. This basically means that given the temperature and the time scale of observation, one can calculate an effective length scale, L_{eff} on which the structures on a surface are in equilibrium with their surroundings and actively changing on the time scale of e.g. STM measurements. Having the E_b energy barrier and L_{eff} at a certain temperature, one can also make at least rough estimates of the effective lengths at other temperatures using this scaling argument. This picture is certainly a result of simplification, as there is a whole set of energy barriers in such a complex physical system as a crystal surface, and the various atomistic mechanisms governed by different barriers freeze out or get activated at different temperatures depending on their corresponding energy barriers.

Comparison or extrapolation to other materials is possible if the energy-barrier set is similar to that of Pb(111). Then the Debye frequency sets the time scale while the energy barriers set the temperature scale, as one can readily deduce it from Eq. (15). On the other hand, if the energy-barrier set is completely different, as for example for Si,[36] it gives rise to a different rate-limiting mechanism namely attachment-detachment for a wide range of temperatures, and such extrapolation is not possible, but a whole set of simulations should be done for the group of materials with this sort of barriers.

VI. CONCLUSIONS

In this paper we deduce energetic and kinetic parameters of a sample metal surface below its roughening temperature. We use kinetic Monte Carlo simulations to mimic the fluctuations of large nanoscale islands on these smooth surfaces in order to determine equilibrium island shapes, anisotropic line tensions in the azimuthal directions of the surface, and the correlation times of the

Fourier modes of the fluctuations.

We derive an analytic expression for the chemical potential of the island edge from the equilibrium island shape and the associated capillary wave fluctuations around it. This chemical potential sets the scale for the anisotropic line tension, [the azimuthal dependence of] which is usually known only up to a multiplicative constant. To account for the anisotropy of the line tension, this procedure contains a transformation from the Fourier modes of the island edge fluctuations to the true eigenmodes. However, detailed analysis of the Fourier and eigen modes of the fluctuations reveals that the transformation to the eigenmodes is unnecessary; at least in our case, the Fourier modes seem to give better results, as gauged by comparison with equipartition.

The obtained line tensions—one of the most important physical parameters of steps on surfaces—are in the correct range compared to known experimental results even in this simplistic model with a rather small set of hopping-energy barriers in the KMC simulation.

The analyses of the correlation times of the Fourier modes show that nanoscale objects fluctuate on the msec time range at moderately high temperatures (400K) on Pb surfaces. Since the atomic processes are activated, this time scale changes dramatically with temperature.

Inclosing, we make a comment on the equilibration time of step structures in Monte Carlo simulations here. The full equilibration of these structures is signalled by the correlation time of the longest wavelength mode, which can be very large (in CPU time) for system sizes and temperatures studied in this paper. To do correct MC measurements *in equilibrium*, one has to pass this time, otherwise results for "equilibrium quantities" can be very misleading as is well known from non-equilibrium statistical mechanics. Without looking at correlation times of Fourier modes it requires very careful analysis to avoid such equilibration problems.[27] Recently, several works have appeared concerning temporal correlation functions, persistence, etc., of steps much longer than ours, and sometimes even several of them, in studies of the interaction between them. They might well suffer from these problems as this equilibration time scales with system size as third or fourth power meaning that a twice

as big system need an order of magnitude longer CPU time to be equilibrated. In the multi-step case a remedy might be that the dynamic exponent may decrease when the steps are really close to each other,[15] but that is apparently rarely the case.

Another comment is due on the measurement of these fluctuations experimentally, which might be difficult because of the above mentioned time scale of the fluctuations. One either has to use techniques with which snapshots of the surface can be taken,[13] or, in direct visualization methods (like STM measurements), the scan rate of the equipment must be faster than the fluctuations of a given wavelength of interest. Otherwise one measures the two ends of a wavelength at such a time separation that they are uncorrelated, which does not make much sense. The "speed" of the fluctuations can be tuned by changing the temperature, but one also has to take into account that lowering the temperature decreases the size of the fluctuations, rendering the measurement harder.

Finally, the extrapolation of our results for nanoobjects to mesoscale features makes possible intriguing comparisons of correlation times of modes of certain wavelengths, and decay or relaxation of larger structures to their equilibrium forms. This comparison reveals a remarkable coincidence in the correlation time of our basically one dimensional features and real three-dimensional objects like a crystallite.

* Corresponding author: szalmaf@physics.umd.edu
† Electronic address: einstein@umd.edu; URL: http://www2.physics.umd.edu/~einstein
[1] For a general introduction to crystal surface phenomena, see A. Pimpinelli and J. Villain, *Physics of Crystal Growth*, (Cambridge Univ. Press, Cambridge, 1998)
[2] For a review of vicinal surfaces, see H.-C. Jeong and E.D. Williams, Surf. Sci. Rep. **34**, 171 (1999)
[3] K. Thürmer, J.E. Reutt-Robey, E.D. Williams, M. Uwaha, A. Emundts, and H.P. Bonzel, Phys. Rev. Lett. **87**, 186102 (2001)
[4] G. Schulze Icking-Konert, M. Giesen, and H Ibach, Phys. Rev. Lett. **83**, 3880 (1999)
[5] S. Dieluweit, H. Ibach, M. Giesen, and T. L. Einstein, Phys. Rev. B **67**, 121410 (2003)
[6] N.C. Bartelt, J.L. Goldberg, T.L. Einstein, E.D. Williams, J. C. Heyraud, and J. J. Métois, Phys. Rev. B **48**, 15453 (1993)
[7] S. Kodambaka, V. Petrova, S. V. Khare, D. Gall, A. Rockett, I. Petrov, and J. E. Greene Phys. Rev. Lett. **89**, 176102 (2002)
[8] S. Kodambaka, S. V. Khare, V. Petrova, D. D. Johnson, I. Petrov, and J. E. Greene, Phys. Rev. B **67**, 035409 (2003)
[9] S.V. Khare and T.L. Einstein, Phys. Rev. B **54**, 11752

(1996)

[10] D.C. Schlösser, L.K. Verheij, G. Rosenfeld, G. Comsa, Phys. Rev. Lett. **82**, 3843 (1999).

[11] S.V. Khare, S. Kodambaka, D. D. Johnson, I. Petrov and J. E. Greene, Surf. Sci. **522**, 75 (2003), a few typographical errors, superfluous term in Eq. (22), and sign problems from Eq. (25a) on

[12] S.V. Khare and T.L. Einstein, Phys. Rev. B **57**, 4782 (1998)

[13] N.C. Bartelt and R.M. Tromp, Phys. Rev. B **54**, 11731 (1996)

[14] A.L. Barabási and H.E. Stanley, *Fractal Concepts in Surface Growth*, (Cambridge Univ. Press, 1995)

[15] A. Pimpinelli, J. Villain, D. E. Wolf, J. J. Métois, J. C. Heyraud, I. Elkinani and G. Uimin, Surf. Sci. **295**, 143 (1993)

[16] G.S. Bales and A. Zangwill, Phys. Rev. B **41**, 5500 (1990)

[17] W.W. Mullins, J. of Appl. Phys. **28**, 333 (1957); **30** 77 (1959)

[18] W.W. Mullins, in *Metal Surfaces: Structure, Energetics and Kinetics* (Am. Soc. Metals, Metals Park, OH, 1963) p. 17.

[19] Landau and Lifshitz, *Statistical Physics*, Part I, Chap. 15, 3rd edition, (Butterworth-Heinemann, 1980)

[20] S. Kodambaka, V. Petrova, S. V. Khare, D. D. Johnson, I. Petrov, and J. E. Greene, Phys. Rev. Lett. **88**, 486101 (2002).

[21] J.G. McLean, B. Krishnamachari, D.R. Peale, E. Chason, J.P. Sethna and B. H. Cooper, Phys. Rev. B **55**, 1811 (1997)

[22] M. Zinke-Allmang, L.C. Feldman and M.H. Grabow, Surf. Sci. Rep. **16**, 377 (1992).

[23] A. B. Bortz, H. M. Kalos and J.L. Lebowitz, J. Comp. Phys. **17**, 10 (1975)

[24] M. E. J. Newman and G. T. Barkema, *Monte Carlo Methods in Statistical Physics* (Clarendon, Oxford, 1999).

[25] M.I. Haftel and M. Rosen, Phys. Rev. B **51**, 4426 (1995); Surf. Sci. **407**, 16 (1998).

[26] H. S. Lim, C. K. Ong, and F. Ercolessi, Surf. Sci. **269/270**, 1109 (1992); http://www.fisica.uniud.it~ercolessi/potentials/Pb/

[27] F. Szalma, W. Selke, and S. Fischer, Physica A **294**, 313 (2001)

[28] A. Karim et al., preprint, Fluctuations of Surface Steps in Equilibrium: A Kinetic Monte Carlo Study

[29] C. Bombis, A. Emundts, M. Novicki, H.P. Bonzel, Surf. Sci. **511**, 83 (2002)

[30] N. C. Bartelt, J. L. Goldberg, T.L. Einstein, and E. D. Williams, Surf. Sci. **273**, 252 (1992).

[31] N. C. Bartelt, T.L. Einstein, and E. D. Williams, Surf. Sci. **312**, 411 (1994).

[32] B. Blagojević and P.M. Duxbury, Phys. Rev. E **60**, 1279 (1999).

[33] N.W. Ashcroft and N.D. Mermin, *Solid State Physics* (Saunders College, Philadelphia, 1976)

[34] L. Kuipers, M.S. Hoogeman, J.W.M. Frenken, and H. van Beijeren, Phys. Rev. B , **52** 11387 (1995)

[35] S. Speller, W. Heiland, A. Biedermann, E. Platzgummer, C. Nagl, M. Schmid, P. Varga, Surf. Sci., **331** 1056 (1995)

[36] J.M. Bermond, J.J. Métois, X. Egéa, and F. Floret, Surf. Sci. **330**, 48 (1995)